ACS APPLIED MATERIALS & INTERFACES

Research Article

www.acsami.org

Organic–Inorganic Hybrid Solution-Processed H_2-Evolving Photocathodes

Lai-Hung Lai,[†] Widianta Gomulya,[†] Matthijs Berghuis,[†] Loredana Protesescu,[‡,§] Remko J. Detz,[∥] Joost N. H. Reek,[∥] Maksym V. Kovalenko,[‡,§] and Maria A. Loi*[,†]

[†]Zernike Institute for Advanced Materials, University of Groningen, Nijenborgh 4, Groningen 9747 AG, The Netherlands

[‡]Department of Chemistry and Applied Biosciences, ETH Zürich, Wolfgang-Pauli-Strasse 10, Zurich 8049, Switzerland

[§]EMPA-Swiss Federal Laboratories for Materials Science and Technology, Überlandstrasse 129, Dübendorf 8600, Switzerland

[∥]Van't Hoff Institute for Molecular Sciences, University of Amsterdam, Science Park 904, 1098 XH Amsterdam, The Netherlands

Supporting Information

ABSTRACT: Here we report for the first time an H_2-evolving photocathode fabricated by a solution-processed organic–inorganic hybrid composed of CdSe and P3HT. The CdSe:P3HT (10:1 (w/w)) hybrid bulk heterojunction treated with 1,2-ethanedithiol (EDT) showed efficient water reduction and hydrogen generation. A photocurrent of −1.24 mA/cm^2 at 0 V versus reversible hydrogen electrode (V_{RHE}), EQE of 15%, and an unprecedented V_{oc} of 0.85 V_{RHE} under illumination of AM1.5G (100 mW/cm^2) in mild electrolyte were observed. Time-resolved photoluminescence (TRPL), internal quantum efficiency (IQE), and transient photocurrent measurements were carried out to clarify the carrier dynamics of the hybrids. The exciton lifetime of CdSe was reduced by one order of magnitude in the hybrid blend, which is a sign of the fast charge separation upon illumination. By comparing the current magnitude of the solid-state devices and water-splitting devices made with identical active layers, we found that the interfaces of the water-splitting devices limit the device performance. The electron/hole transport properties investigated by comparing IQE spectra upon front- and back-side illumination evidenced balanced electron/hole transport. The Faradaic efficiency is 80–100% for the hybrid photocathodes with Pt catalysts and ∼70% for the one without Pt catalysts.

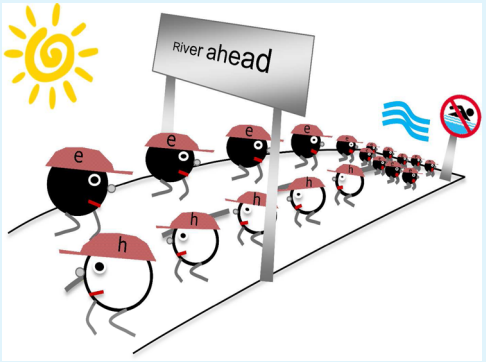

KEYWORDS: *photoelectrochemical water splitting, photocathode, H_2 generation, organic–inorganic hybrids, colloidal nanocrystal*

1. INTRODUCTION

Hydrogen (H_2) is one of the most promising fuels for the 21st century owing to its high energy density and clean reaction products ($2H_2 + O_2 \rightarrow 2H_2O$). Currently, most H_2 is produced by steam-reforming of fossil fuels. In the framework of the development of cleaner renewable energies, solar-to-H_2 production has attracted significant attention in the last 40 years, since Honda and Fujishima first demonstrated photocatalytic water splitting by employing TiO_2 as a photoanode and Pt as a cathode.[1] Recently, Yang et al.[2] demonstrated over 90% external quantum efficiency (EQE) using a hierarchical nanostructured array of TiO_2. Nevertheless, because of the wide band gap characteristic of TiO_2, the photoconversion efficiency of this device is limited to 1.13% at 0.51 V vs reversible hydrogen electrode (V_{RHE}) under illumination of AM1.5G (100 mW/cm^2).

To harvest a broader portion of the solar spectrum, narrow-band gap semiconductors such as CdSe, CdTe, and PbS, especially in their nanocrystal (NC) form, have been employed as photoanodes interfaced with mesoporous TiO_2.[3−9] However, most of these materials are not stable under a water oxidation environment because of their energy levels and thermodynamic properties. In fact, the excited carriers (electrons and holes) might react either with water or the anode materials themselves, depending on the thermodynamics and kinetics of these reactions.

Several approaches have been employed to avoid photocorrosion of the electrode material. For example, a sacrificial electrolyte is often necessary for the II–VI NCs, such as CdSe, CdS, PbS, and CdTe.[8−11] This sacrificial electrolyte acts as a hole scavenger, which prevents the oxidation of the NCs. Not only NCs but also bulk semiconductors have serious problems of photocorrosion. Recently, Hu et al.[12] reported remarkable passivation of Si, GaAs, and GaP photoanodes by amorphous TiO_2 coatings (4–143 nm) deposited by atomic layer deposition (ALD). Paracchino et al.[13] reported that a monolayer of Al-doped zinc oxide and titanium oxide also protects Cu_2O photocathodes from decomposition.

Another strategy to avoid photocorrosion is to select materials for which this phenomenon is energetically less

Received: May 25, 2015
Accepted: August 11, 2015
Published: August 11, 2015

DOI: 10.1021/acsami.5b04550
ACS Appl. Mater. Interfaces 2015, 7, 19083–19090

favorable than the water reduction or oxidation. This is the case for CdSe, for which the photocathodic decomposition energy level is higher than the proton reduction energy. Thus, CdSe QDs are candidates for stable proton reduction. In principle, the ~0.8 eV energy difference between the conduction band of CdSe and the ideal proton reduction potential should provide enough voltage to drive proton reduction. Recently, well-dispersed CdSe and CdTe NCs anchored with cocatalysts have been demonstrated as a promising homogeneous photocatalytic proton reduction system in a sacrificial electrolyte.[14,15]

A truly new approach for proton reduction was reported by Bourgeteau et al.,[16] which employed an organic (P3HT:PCBM) bulk heterojunction (BHJ) with MoS_3 cocatalyst in strong acid electrolyte. In this device, holes travel to the indium tin oxide (ITO) electrodes, and electrons are directed to the solid/liquid interface for proton reduction. Unfortunately, the instability of this all-organic photocathode in the electrolyte inhibits the application of this strategy.

In this work, organic–inorganic hybrid solution-processed BHJ electrodes are demonstrated as low-cost and high-efficiency photocathodes. The photoelectrochemical (PEC) cell fabricated with a hybrid film coated with Pt as cocatalyst shows efficient water reduction with an EQE up to 15%, a photocurrent of -1.24 mA/cm^2 at 0 V_{RHE}, and an unprecedented open-circuit voltage of 0.85 V_{RHE} under illumination of AM1.5G (100 mW/cm^2) in pH 7 phosphate buffer. The Faradaic efficiency was determined to be 100% in the beginning of functioning and stabilized at 80% after 0.5 h. Time-resolved photoluminescence (TRPL) shows that the long exciton lifetime of CdSe is strongly reduced in the blend, indicating a fast charge separation upon illumination. The IQE spectra measured by illuminating the photocathodes from front- and back-side evidence balanced electron/hole transport. The considerable decay of the photocurrent after switching the illumination off and the absence of anodic spikes in the photocurrent after switching the light on show that electron transfer/trapping is the main mechanism limiting the photocathodes in absence of Pt catalyst. When the platinum catalyst is deposited on the photocathode, an almost ideal carrier transport without any serious carrier recombination is revealed.

2. RESULTS AND DISCUSSION

Reactions 1–4 show the four possible pathways for excited carriers in CdSe nanocrystals when they are in contact with water.

$$2H^+ + 2e^- \rightarrow H_2 \quad (1)$$

$$O_2 + 4H^+ + 4e^- \rightarrow 2H_2O \quad (2)$$

$$CdSe \rightarrow Cd^{2+} + Se + 2e^- \text{ (oxidation)} \quad (3)$$

$$CdSe + 2e^- \rightarrow Cd + Se^{2-} \text{ (reduction)} \quad (4)$$

The relative energy levels of these reactions with respect to the energy level of photoanodic decomposition are shown in Figure 1a, where the topmost energy level of the scale is the vacuum level at 0 eV. For CdSe, the photoanodic decomposition energy ($E_{p,dec}$) is lower than that of the water oxidation energy (E_{H_2O/O_2}), resulting in a higher priority for photocorrosion with respect to water oxidation.[17–19] In comparison to TiO_2, the energy level of photoanodic decomposition ($E_{p,dec}$) is higher (Figure 1a) than that of water oxidation (E_{H_2O/O_2}), thus stable photocatalytic water

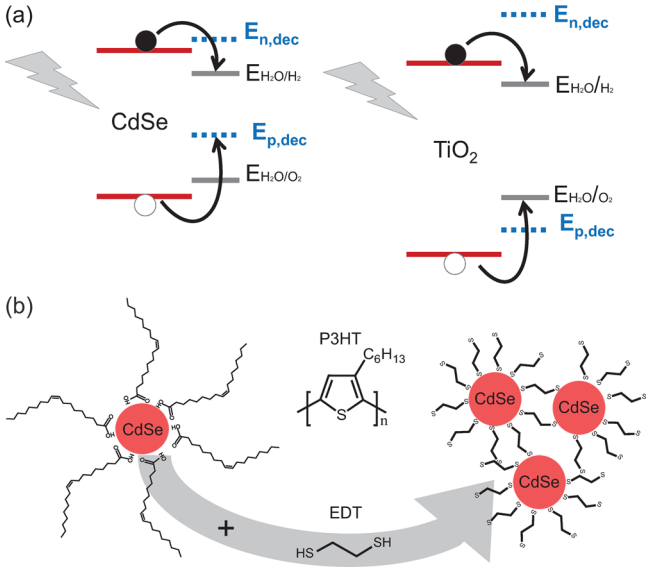

Figure 1. (a) Schematic energy diagram of CdSe and TiO_2; the energy levels for water oxidation, proton reduction, and photodecomposition for the active materials are also shown. $E_{n,dep}$ and $E_{p,dep}$ represent the decomposition potential of the materials for reactions with electrons and holes, respectively. (b) Chemical structure of P3HT and EDT; schematics of CdSe NC with oleic acid ligands and after cross-linking using EDT.

splitting can be observed. However, in both TiO_2 and CdSe, the photocathodic decomposition energy ($E_{n,dec}$) is higher than the proton reduction energy (E_{H_2O/H_2}). Therefore, stable proton reduction is possible in both materials.

We used CdSe NCs as active material for photocatalytic proton reduction, combining it with a conjugated polymer to form a type-II heterojunction. Ideally, the nanostructured inorganic–organic blend allows efficient charge separation upon illumination if the HOMO and LUMO of the two materials are staggered (type-II heterojunction). In this photocathode, unlike the bulk n-CdSe electrodes, the disappearance of the band bending should allow easier electron transfer to the solid/liquid interface.

Figure 1b shows the chemical structure of P3HT, 1,2-ethanedithiol (EDT), and a schematic of CdSe NCs. The CdSe NCs are encapsulated with long, insulating oleic acid molecules, which allow for a stable colloidal solution by hindering the NCs aggregation. CdSe NCs with a diameter of 3.7 nm were used, which have a band gap of about 2 eV. The size of CdSe NCs is calculated according to the first absorption peak in the solution.[20] As reported in recent literature,[21–23] CdSe and P3HT form a type-II heterojunction (Figure S1b), which should guarantee a fast charge separation upon illumination. However, the native insulating property and the length of the oleic acid ligands limit the carrier transport. EDT has been reported to effectively replace oleic acid and to functionalize the surface of PbS, PbSe, and CdSe NCs, lowering the distance between them and therefore allowing charge transport.[24–28]

To understand the carrier dynamics in the hybrid photocathode, steady-state PL and TRPL measurements were carried out. P3HT and QDs hybrid films were spin-cast on quartz substrates using the same parameters used for fabrication of the hybrid photocathode, whereas the films of CdSe with oleic acid ligands (OA) were deposited by drop-casting. Figure 2a shows the steady-state photoluminescence of pure P3HT, CdSe (OA),

DOI: 10.1021/acsami.5b04550
ACS Appl. Mater. Interfaces 2015, 7, 19083–19090

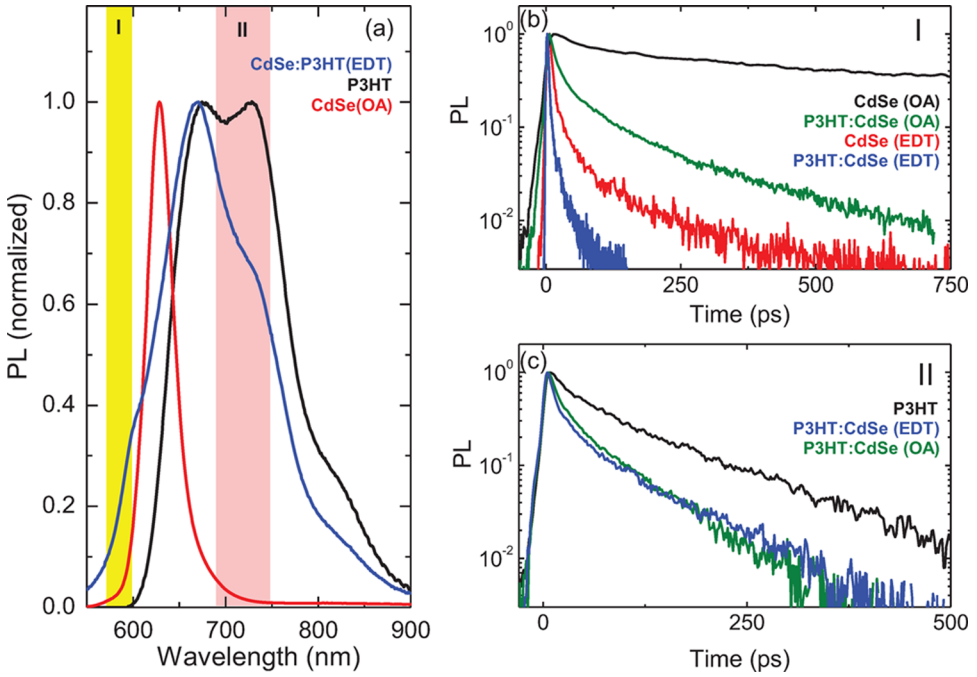

Figure 2. (a) Normalized steady-state PL spectra of pure P3HT, CdSe (OA); and hybrid film after EDT treatment. (b) Time-resolved PL of CdSe (OA), P3HT:CdSe (OA), CdSe (EDT), and P3HT:CdSe (EDT) measured in the wavelength range indicated by the yellow stripe in a, and (c) that of the same samples measured in the wavelength range indicated by the red stripe in a.

and the hybrid film after EDT treatment. The CdSe (OA) sample has an emission peak at ∼628 nm, whereas P3HT shows its typical vibronic progression with peaks centered at ∼660 and ∼710 nm.[29] Compared to pure P3HT, the hybrid film shows an additional emission below 600 nm, which is ascribed to the CdSe NCs. A different relative intensity of the P3HT peaks is also observed. This is due to the lack of aggregation in the hybrid films determined by the intermixing of the CdSe NCs in between the polymer chains, making the PL contribution of the P3HT look more similar to the P3HT spectra in solution.[29]

The dynamics of the PL for CdSe (OA), P3HT:CdSe (OA), CdSe (EDT), and P3HT:CdSe (EDT) are shown in Figure 2b,c. Figure 2b shows the data measured below 600 nm (yellow region in Figure 2a), which is ascribed to the exciton recombination in the NCs. The relatively long lifetime (45 ps (τ_1) and 667 ps (τ_2)) of CdSe (OA) film (black line) shows the confinement of the photoexcited excitons in CdSe NCs with long insulating ligands. After EDT treatment (red line), the lifetime of the NCs emission becomes one order of magnitude shorter (6 ps (τ_1) and 43 ps (τ_2)), resulting from the partial loss of confinement, which allows the opening of new non-radiative channels. The CdSe:P3HT blend (green line) also shows shorter lifetime (12 ps (τ_1) and 96 ps (τ_2)) compared to that of CdSe (OA) film, indicating the formation of a type-II heterojuncition in the blend. After EDT treatment of the hybrid film (blue line), the lifetime becomes extremely short (3 ps (τ_1) and 25 ps (τ_2)), showing the fast charge separation upon illumination. It is important to underline that at least for what concerns τ_1, these last lifetimes are limited by the time resolution of the experimental setup.

The PL decays of the emission above 600 nm (red region in Figure 2a) are shown in Figure 2c. The PL in this range is attributed to the dynamics of the photoexcited excitons in P3HT. The shorter lifetimes of the hybrid blend sample (13 ps (τ_1) and 74 ps (τ_2)) compared to those of the pristine polymer (27 ps (τ_1) and 134 ps (τ_2)) indicate as previously a faster charge separation in the blend, which is explained in terms of the formation of a type-II heterojunction between CdSe NCs and P3HT. In this case, after EDT ligand exchange, the exciton lifetime in P3HT shows minimum variation, evidencing the lack of influence of the ligand exchange for the charge transfer from P3HT to the NCs. This interesting finding implies that in the case of the CdSe emission the fastened dynamics upon EDT treatment are related primarily to a better inter-NC transfer, which is quite plausible considering the limited amount of polymer present in the thin film.

To further prove the formation of a type-II heterojunction, we first fabricated solar cells using this hybrid thin film with different polymer/NCs ratios, as shown in Figure S1a. Devices were completed with a cathode composed by LiF/Al, which was vacuum-evaporated (energy diagram in Figure S1b). Figure S1c,d shows the current density−voltage characteristics (J−V) and EQE spectra of devices fabricated with two different NC to polymer ratios. The hybrid CdSe/P3HT films show a V_{oc} approaching 0.8 V and a photocurrent density of the CdSe/P3HT 10:1 (w/w) ratio that is two times higher than the one of the 5:1 (w/w) ratio. Recently, Kwon et al.[30] reported the inhomogeneous distribution of CdSe and P3HT in similar hybrid film by X-ray photoelectron spectroscopy (XPS), showing that CdSe concentrates near the bottom surface whereas P3HT is located at the top surface. Therefore, more CdSe is necessary for efficient electron transport, which explains why the 10:1 (w/w) CdSe:P3HT sample shows higher efficiency than the 5:1 (w/w) CdSe:P3HT one. The EQE spectra of the hybrid film with 10:1 (w/w) ratio shows photon-to-electron conversion values up to ∼50% and clear signature in the photocurrent of the CdSe NCs excitonic peak.

The optimized hybrid film was deposited on a fluorine-doped tin oxide (FTO)/Cr/Au substrate to be used as a proton

DOI: 10.1021/acsami.5b04550
ACS Appl. Mater. Interfaces 2015, 7, 19083−19090

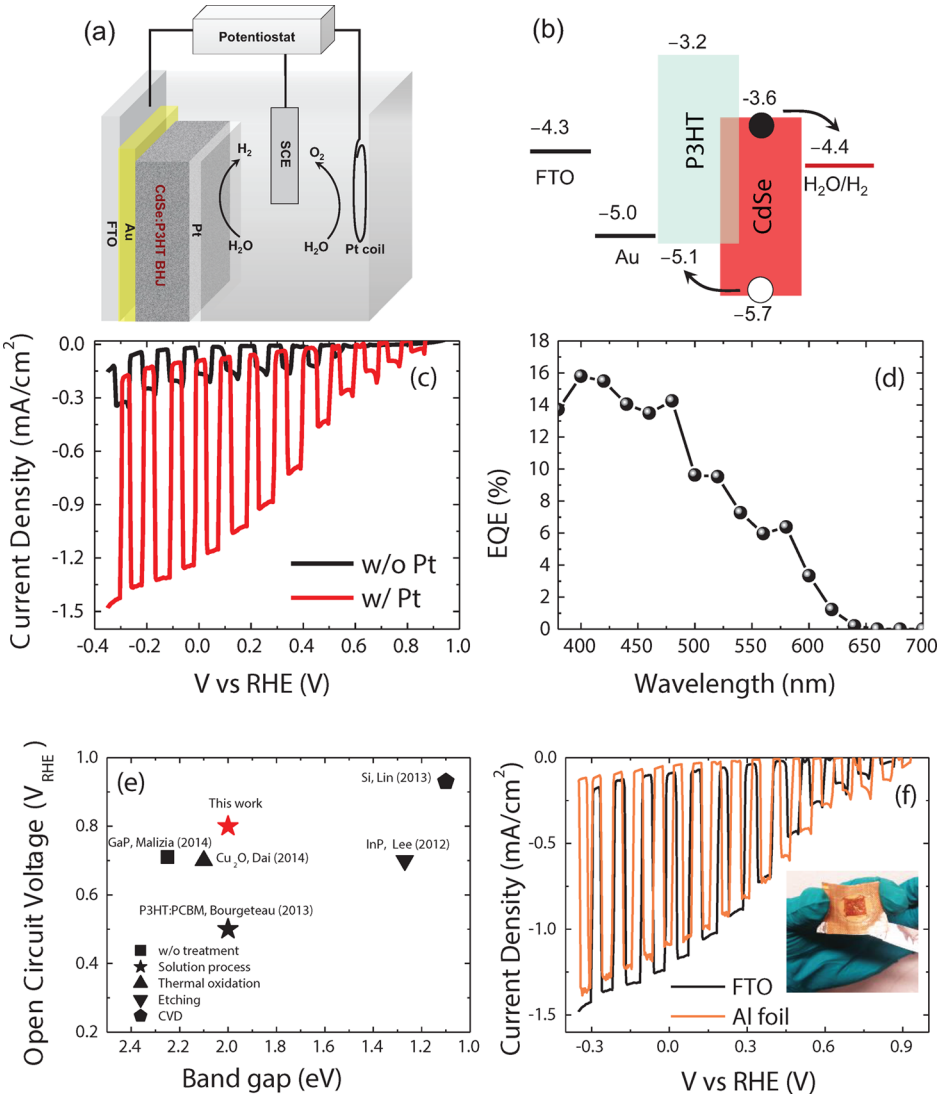

Figure 3. (a) Schematic of hybrid water-splitting electrochemical cell. (b) Energy diagram of the hybrid photocathode. (c) $J-V$ curves of hybrid photocathodes without Pt (black line) and with Pt (red line). (d) EQE spectrum of the photocathode with Pt deposition. (e) Benchmark of open circuit voltages and band gap of the most important materials for H_2-evolving photocathodes; the deposition technique and eventual special treatments are indicated by the symbols.[16,31−34] (f) $J-V$ characteristics of hybrid photocathodes on FTO (black line) and Al foil (orange line). The inset shows a photo of the flexible photocathode on Al foil substrate.

reduction photocathode. A thin Pt layer was electrodeposited on top of the active layer to act as proton reduction catalyst. The photocathodes were measured in a three-electrode electrochemical cell, which is schematically illustrated in Figure 3a. Figure 3b shows the energy levels of the materials used in the photocathode.

Figure 3c,d shows the $J-V$ curves and EQE spectra of the hybrid photocathodes, respectively. The $J-V$ characteristic measured under chopped light shows a clear photocurrent contribution under AM1.5G (100 mW/cm^2) illumination in a mild electrolyte (0.1 M phosphate buffer, pH 7). After Pt deposition, the photocurrent increases from −0.16 to −1.24 mA/cm^2 and the V_{oc} increases from 0.55 to 0.85 V_{RHE}, which is the highest reported value for the solution-processed single-junction photocathode up to now. A summary of the photovoltages recently reported with various materials and fabrication methods is displayed in Figure 3e.[16,31−34]

The photocurrent measured (−1.24 mA/cm^2 at 0 V_{RHE}) is substantially higher than the one reported for the previously mentioned all-organic (P3HT:PCBM) film with TiO_2/MoS_3 (−0.2 mA/cm^2 at 0 V_{RHE}) and with TiO_2/Pt (∼1 mA/cm^2 at 0 V_{RHE}).[16,35] However, compared to our solid-state hybrid solar cells (Figure S1c), the photocurrent is four times lower; a difference that can be reasonably ascribed to a problem at the interface with water. Here, it is important to notice that for the proton reduction photocathode an electrodeposited Pt layer is used to extract the electrons whereas in the solar cell an aluminum electrode is acting as cathode. The EQE spectra of the photocathode with Pt catalyst measured at 0 V_{RHE} (Figure 3d) shows a photon-to-electron efficiency up to 15% between 400 and 475 nm. The theoretical short-circuit current obtained by AM 1.5G-weighted integration of the EQE spectrum is 1.22 mA/cm^2, which is less than 2% lower than the current obtained in the $J-V$ measurement.

The Faradaic efficiency of the system is obtained by measuring the H_2 generation volume with in situ gas chromatography (GC), and estimating the volume ideally

DOI: 10.1021/acsami.5b04550
ACS Appl. Mater. Interfaces 2015, 7, 19083−19090

generated from the photocurrent using the following equations. (The schematic of the GC set up is reported in Figure S2).

$$V_{H_2}(\text{ideal}) = \frac{Q}{2F} \times 24.5\ (\text{L})$$

$$\text{FE}\ (\%) = \frac{V_{H_2}(\text{measured})}{V_{H_2}(\text{ideal})} \times 100\%$$

where Q is the total charge and F is the Faraday constant (96 500 C/mol) for 1 mol of gas at standard conditions of temperature and pressure (25 °C and 1 atm) that occupies 24.5 L. Figure 4a shows the measured and ideal H_2-evolving volume

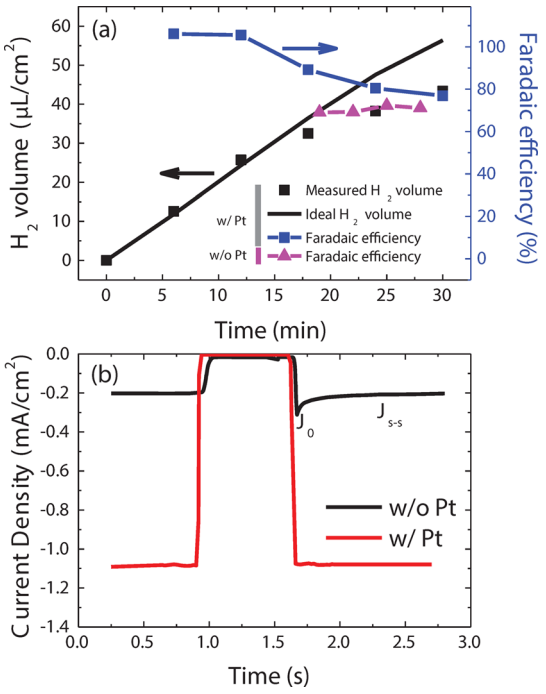

Figure 4. (a) Measured and ideal H_2 generation volume at 1 atm and 25 °C. The calculated Faradaic efficiency for both cathodes with and without Pt catalyst is represented by blue and pink symbols, respectively. (b) Transient photocurrent measurement for the electrode with and without Pt measured at 0 V_{RHE}.

and the corresponding calculated Faradaic efficiency (FE) for the hybrid photocathode measured at 0 V_{RHE}. The hybrid photocathodes without Pt catalysts show an FE of ~70%, whereas the FE of the photocathode with the Pt catalysts reaches 80−100%. The H_2-bubbling process is shown in the Supporting Information video. The photocathode was also fabricated on flexible Al foil showing, similar characteristics as the one reported for the rigid substrate (Figure 3f), illustrating the potential of this hybrid blend for a low-fabrication-cost artificial leaf.

To further understand the charge transfer dynamics in the photocathode, the hybrid films were deposited on ITO/PEN substrates (Pt not deposited on these samples); this fully transparent electrode allows front- and back-side illumination (Figure S3). Under front-side illumination, most charge carriers (electrons and holes) are generated at the solid/liquid interface. In this case, holes need to diffuse a longer distance before being collected by the respective electrode, whereas electrons have shorter traveling distance to reach the solid/liquid interface. The dependence of the internal quantum efficiency (IQE) on the illumination direction gives an indication of the transport limits of either electrons or holes in the device. To obtain the IQE spectra, it is necessary first to measure the EQE spectra (Figure S3a). The EQE measured from the back-side illumination gives lower values compared to that from the front-side illumination because of the light absorption by the substrates. The IQE spectra are estimated by normalizing the EQE with the total photon absorption in the hybrid active layer. (Substrate absorption is considered only in the back-side illumination, reflection losses are not considered.) Figure S3b shows that the estimated IQE values for front- and back-side illumination are practically identical; therefore, we can deduce that the hole and electron transport are balanced.

The carrier transport dynamics for samples with and without Pt were characterized by transient photocurrent measurements reported in Figure 4b. Transient photocurrent measurements were conducted at 0 V_{RHE} with a shutter opening and closing every 500 ms. When the light is switched on, the transient photocurrent of the cathode without Pt catalyst shows a step-like rise of the current until a level J_0, which tends to decrease toward the steady-state current $J_{s\text{-}s}$. The difference between the current density J_0 and $J_{s\text{-}s}$ can be ascribed to charge recombination. The recombination can be due to either the accumulation/trapping of holes/electrons in the bulk or the accumulation/trapping of holes/electrons at the interface. If hole trapping/accumulation dominates, then the anodic current contribution from the recombination of majority carrier (in this case, electrons) in CdSe should arise after the light is switched off. However, in our measurements, an absence of anodic transient current was observed, indicating that the accumulation/trapping of hole can be ruled out in this system. Thus, electron trapping/accumulation is the main recombination mechanism.[36−38] This is further demonstrated by the optimized photocathode with Pt catalyst (Figure 4b), which shows an ideal transient photocurrent behavior resembling a step function.

The stability of the hybrid photocathode is reported in Figure 5a,b. The photocurrent appears stable without any decay within 1 h; even after refilling of the electrolyte, the same value of photocurrent is measured (Figure 5a). In Figure 5a, the decay of the photocurrent during light chopping is caused by the accumulation of bubbles at the surface of the photocathode, which makes the effective active area smaller.

The long-term stability of the hybrid photocathode is reported in Figure 5b. For this measurement, the device was measured continuously for 16 h. In the first half hour, the device shows an increase of the performance; the current after reaching its maximum value starts to decrease after about 2 h of functioning. Interestingly, the fresh sample shows almost an ideal transient photocurrent with step function behavior (inset of Figure 5b), whereas the degraded photocathode (after 16 h of continuous functioning) shows a fast decay of the photocurrent after the light is switched on, which as we discussed previously is a clear indication of electron accumulation at the solid/liquid interface. This data indicates that either the catalyst activity is compromised (poisoning) or the CdSe is degraded after long functioning times. The analysis of the photocathode after 16 h functioning allows us to exclude the detachment of the Pt layer. To further improve the long-term stability of the photocathode, a possible strategy would be to protect it with an oxide interlayer, which acts as tunnelling barrier for electrons but protects the active layer from the water environment.

DOI: 10.1021/acsami.5b04550
ACS Appl. Mater. Interfaces 2015, 7, 19083−19090

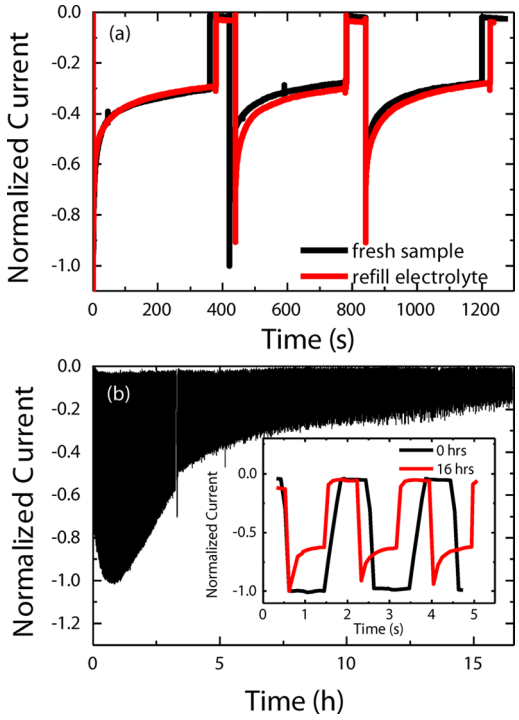

Figure 5. (a) Photocurrent stability measurement of the hybrid photocathodes after stabilization of the sample at 0 V_{RHE}: fresh sample (black line) and sample after refill of electrolyte (red line). (b) Long-term stability for the optimized sample. The inset shows the transient photocurrent for fresh samples and samples after 16 h measurements.

3. CONCLUSIONS

We reported for the first time an H_2-evolving photocathode fabricated by solution-processed organic−inorganic hybrids composed of CdSe and P3HT. The CdSe:P3HT hybrid bulk heterojunction treated with 1,2-ethanedithiol (EDT) showed efficient water reduction and hydrogen generation. A photocurrent of −1.24 mA/cm^2 at 0 V_{RHE}, EQE of 15%, and an unprecedented V_{oc} of 0.85 V_{RHE} under illumination of AM1.5G (100 mW/cm^2) in mild electrolyte were observed. The Faradaic efficiency is 80−100% for the hybrid photocathodes with Pt catalysts and ∼70% for the one without Pt catalysts.

In this way, we demonstrated that n-type NCs can be used as photocathodes for proton reduction. This is a new route to fabricate stable photocathodes with materials that are not stable in water oxidation environment but that can eventually be stable in a proton reduction environment. In future, this strategy could be extended to NCs having smaller band gaps and containing nontoxic elements. Furthermore, higher stability could be achieved by using oxides as interlayers.

4. EXPERIMENTAL SECTION

4.1. CdSe Nanocrystal Synthesis. The synthesis of CdSe NCs was adopted from ref 17. To prepare the Cd-myristate precursor, cadmium nitrate (1.542 g, 5 mmol in 150 mL methanol) was added dropwise to sodium hydroxide (0.6 g, 15 mmol) and myristic acid (3.42 g, 15 mmol) in methanol (500 mL). The resulting white precipitate was washed with methanol three times and then dried overnight at ∼60 °C under vacuum. CdSe NCs were then synthesized by combining cadmium myristate 1.132 g (2 mmol), SeO_2 (2 mmol), and ODE (128 mL) in a 500 mL three-necked flask. The resulting mixture was degassed under vacuum (∼50 mTorr, 10 min) at room temperature. Under argon flow and with magnetic stirring, the mixture was heated to the reaction temperature (240 °C) at a rate of 20 °C/min. After 3 min at 240 °C, 4 mL of oleic acid was injected, and the mixture was cooled to RT. ODE was distilled from crude solution at 155 °C under vacuum until 20 mL of solvent remained in the flask. The particles were washed 3 times with hexane as solvent and ethanol as nonsolvent.

4.2. Hybrid Solar Cell Fabrication. ITO substrates were cleaned with soap and water and sonicated in deionized (DI) water, acetone, and isopropyl alcohol in an ultrasonic bath for each cleaning step. The CdSe NCs were mixed with P3HT (Plexcore OS 2100, regioregular, average M_n = 54 000−75 000) in chloroform with different weight ratio, where the CdSe NCs sustain 30 mg/mL. The hybrid film was spin-coated on ITO by 1000 rpm for 1 min. The 1% EDT solution in acetonitrile (v/v) was drop-cast and left to react on the hybrid film for 1 min before spin-drying. The samples were further rinsed with acetonitrile and spin-dried. After fabrication, the devices were annealed at 110 °C for 20 min. Consequently, 1 nm of LiF and 100 nm of Al were deposited on the hybrid film by vacuum evaporation.

4.3. Hybrid Photocathode Fabrication. FTO substrates were cleaned with the same procedure used for ITO, then 5 nm of Cr and 100 nm of Au film were evaporated on FTO. For transparent flexible photocathode, the ITO/polyethylene naphthalate (PEN) substrates (Visiontek Systems Ltd., sheet resistance < 15 ohm/sq) were cleaned by 10 min sonication in acetone. The hybrid film was spin-casted on the substrates as reported for the hybrid solar cells above. Pt was deposited on top of the hybrid layer by electrodeposition in 5 mM $H_2PtCl_6{\cdot}6H_2O$ aqueous solution with a pH value of 11 tuned by 2 M NaOH at potential of −0.627 V vs SCE for 10 min. No Pt catalyst was deposited on the transparent photocathode in order to enable investigation of the EQE under illumination from both the front- and back-side.

4.4. Characterization. *I*−*V* curves were measured with a SP-200 Bio-Logic potentiostat equipped with an electrochemical impedance spectroscopy analyzer. Solar cell measurements were carried out under 100 mW/cm^2 AM 1.5G conditions obtained with a solar simulator (SF150 class A, Sciencetech) calibrated by a Si reference cell (SRC-1000-RTD-QZ, VLSI Standards Incorporated). EQE measurements were carried out at short-circuit voltage using a 250 W quartz tungsten halogen lamp (6334NS, Newport with lamp housing 67009, Newport), and wavelength selection was obtained with a set of band-pass filters (Thorlabs) with full width at half maximum (fwhm) = 10 ± 2 nm from 400 to 740 nm. PD300 (Ophir Optics) was used as calibrated photodiodes. The IQE spectra reported in the Supporting Information are estimated from the EQE spectra using the absorption of the active layer and of the substrate.

The photocathode was characterized by a three-electrode electrochemical cell composed of a working electrode, reference electrode (saturated calomel electrode (SCE)), and counter electrode (Pt coil) in 0.1 M NaH_2PO_4 phosphate buffer with a pH value of 7 tuned by 2 M NaOH. The electrolyte was degassed by bubbling into it dry N_2 for 30 min before PEC measurements were taken. The PEC cell was connected to a Compact GC from InterScience 5 Å molsieve paraplot column with TCD detector. The headspace gas was continuously pumped through the system with a N68ST.18 membrane pump with a PTFE-coated membrane and PTFE valve plate, purchased from KNF Verder B.V. The film thickness measurements were carried out using a Veeco Dektak 6 M profilometer. Photoluminescence measurements were carried out by exciting the samples at 400 nm by the second harmonic of a mode-locked Ti:sapphire laser delivering pulses of 150 fs at a repetition frequency of 76 MHz. The steady-state PL was recorded using a Si CCD detector, whereas TRPL measurements were recorded by a Hamamatsu streak camera working in synchroscan mode. All PL spectra were corrected for the spectral response of the setup.

■ ASSOCIATED CONTENT

Supporting Information

The Supporting Information is available free of charge on the ACS Publications website at DOI: 10.1021/acsami.5b04550.

DOI: 10.1021/acsami.5b04550
ACS Appl. Mater. Interfaces 2015, 7, 19083−19090

Solid-state solar cells. Schematic drawing of in situ GC-PEC setup. (PDF)

Bubble generation on the photocathode under the light. (AVI)

AUTHOR INFORMATION

Corresponding Author

*E-mail: M.A.Loi@rug.nl. Tel.: +31 50 3634119. Fax: +31 50 3638751.

Notes

The authors declare no competing financial interest.

ACKNOWLEDGMENTS

We acknowledge the generous financial support from Foundation for Fundamental Research on Matter (FOM) for the project "Towards bio-solar cells" (FOM15) and from the Zernike Institute for Advanced Materials. The authors also express thanks to A. Kamp, R. Gooijaarts, and J. Baas for technical support, and finally to Prof. J. J. Wu, Prof. J. S. Chen, J. S. Yang, and H. C. Chen for discussion. Additionally, L. H. Lai thanks Delta Electronics for the support.

REFERENCES

(1) Fujishima, A.; Honda, K. Electrochemical Photolysis of Water at a Semiconductor Electrode. *Nature* **1972**, *238* (5358), 37−38.

(2) Yang, J. S.; Liao, W. P.; Wu, J. J. Morphology and Interfacial Energetics Controls for Hierarchical Anatase/Rutile TiO_2 Nanostructured Array for Efficient Photoelectrochemical Water Splitting. *ACS Appl. Mater. Interfaces* **2013**, *5* (15), 7425−7431.

(3) Luo, J.; Ma, L.; He, T.; Ng, C. F.; Wang, S.; Sun, H.; Fan, H. J. TiO_2/(CdS, CdSe, CdSeS) Nanorod Heterostructures and Photoelectrochemical Properties. *J. Phys. Chem. C* **2012**, *116* (22), 11956−11963.

(4) Luo, J.; Karuturi, S. K.; Liu, L.; Su, L. T.; Tok, A. I.; Fan, H. J. Homogeneous Photosensitization of Complex TiO_2 Nanostructures for Efficient Solar Energy Conversion. *Sci. Rep.* **2012**, *2*, 451 DOI: 10.1038/srep00451.

(5) Hensel, J.; Wang, G.; Li, Y.; Zhang, J. Z. Synergistic Effect of CdSe Quantum Dot Sensitization and Nitrogen Doping of TiO_2 Nanostructures for Photoelectrochemical Solar Hydrogen Generation. *Nano Lett.* **2010**, *10* (2), 478−483.

(6) Trevisan, R.; Rodenas, P.; Gonzalez-Pedro, V.; Sima, C.; Sanchez, R. S.; Barea, E. M.; Mora-Sero, I.; Fabregat-Santiago, F.; Gimenez, S. Harnessing Infrared Photons for Photoelectrochemical Hydrogen Generation. A PbS Quantum Dot Based "Quasi-Artificial Leaf. *J. Phys. Chem. Lett.* **2013**, *4* (1), 141−146.

(7) Lee, J. W.; Son, D. Y.; Ahn, T. K.; Shin, H. W.; Kim, I. Y.; Hwang, S. J.; Ko, M. J.; Sul, S.; Han, H.; Park, N. G. Quantum-Dot-Sensitized Solar Cell with Unprecedentedly High Photocurrent. *Sci. Rep.* **2013**, *3*, 1050 DOI: 10.1038/srep01050.

(8) Lai, L. H.; Gomulya, W.; Protesescu, L.; Kovalenko, M. V.; Loi, M. A. High Performance Photoelectrochemical Hydrogen Generation and Solar Cells with a Double Type II Heterojunction. *Phys. Chem. Chem. Phys.* **2014**, *16* (16), 7531−7537.

(9) Lai, L. H.; Protesescu, L.; Kovalenko, M. V.; Loi, M. A. Sensitized Solar Cells with Colloidal PbS-CdS Core-Shell Quantum Dots. *Phys. Chem. Chem. Phys.* **2014**, *16* (2), 736−742.

(10) Gerischer, H. On the Stability of Semiconductor Electrodes Against Photodecomposition. *J. Electroanal. Chem. Interfacial Electrochem.* **1977**, *82* (1−2), 133−143.

(11) Brown, K. A.; Wilker, M. B.; Boehm, M.; Dukovic, G.; King, P. W. Characterization of Photochemical Processes for H_2 Production by CdS Nanorod-[FeFe] Hydrogenase Complexes. *J. Am. Chem. Soc.* **2012**, *134* (12), 5627−5636.

(12) Hu, S.; Shaner, M. R.; Beardslee, J. A.; Lichterman, M.; Brunschwig, B. S.; Lewis, N. S. Amorphous TiO_2 Coatings Stabilize Si, GaAs, and GaP Photoanodes for Efficient Water Oxidation. *Science* **2014**, *344* (6187), 1005−1009.

(13) Paracchino, A.; Laporte, V.; Sivula, K.; Gratzel, M.; Thimsen, E. Highly Active Oxide Photocathode for Photoelectrochemical Water Reduction. *Nat. Mater.* **2011**, *10* (6), 456−461.

(14) Li, Z.-J.; Li, X.-B.; Wang, J.-J.; Yu, S.; Li, C.-B.; Tung, C.-H.; Wu, L.-Z. A Robust "Artificial Catalyst" *in situ* Formed from CdTe QDs and Inorganic Cobalt Salts for Photocatalytic Hydrogen Evolution. *Energy Environ. Sci.* **2013**, *6* (2), 465−469.

(15) Das, A.; Han, Z.; Haghighi, M. G.; Eisenberg, R. Photogeneration of Hydrogen from Water Using CdSe Nanocrystals Demonstrating the Importance of Surface Exchange. *Proc. Natl. Acad. Sci. U. S. A.* **2013**, *110* (42), 16716−16723.

(16) Bourgeteau, T.; Tondelier, D.; Geffroy, B.; Brisse, R.; Laberty-Robert, C.; Campidelli, S.; de Bettignies, R.; Artero, V.; Palacin, S.; Jousselme, B. A H_2-Evolving Photocathode Based on Direct Sensitization of MoS_3 with an Organic Photovoltaic Cell. *Energy Environ. Sci.* **2013**, *6* (9), 2706−2713.

(17) Bak, T.; Nowotny, J.; Rekas, M.; Sorrell, C. C. Photo-Electrochemical Hydrogen Generation from Water Using Solar Energy. Materials-Related Aspects. *Int. J. Hydrogen Energy* **2002**, *27* (10), 991−1022.

(18) Chen, S.; Wang, L.-W. Thermodynamic Oxidation and Reduction Potentials of Photocatalytic Semiconductors in Aqueous Solution. *Chem. Mater.* **2012**, *24* (18), 3659−3666.

(19) Berardi, S.; Drouet, S.; Francas, L.; Gimbert-Surinach, C.; Guttentag, M.; Richmond, C.; Stoll, T.; Llobet, A. Molecular Artificial Photosynthesis. *Chem. Soc. Rev.* **2014**, *43* (22), 7501−7519.

(20) Jasieniak, J.; Smith, L.; Embden, J. v.; Mulvaney, P.; Califano, M. Re-examination of the Size-Dependent Absorption Properties of CdSe Quantum Dots. *J. Phys. Chem. C* **2009**, *113* (45), 19468−19474.

(21) Wang, X.; Song, W.; Liu, B.; Chen, G.; Chen, D.; Zhou, C.; Shen, G. High-Performance Organic-Inorganic Hybrid Photodetectors Based on P3HT:CdSe Nanowire Heterojunctions on Rigid and Flexible Substrates. *Adv. Funct. Mater.* **2013**, *23* (9), 1202−1209.

(22) Fu, W.; Shi, Y.; Qiu, W.; Wang, L.; Nan, Y.; Shi, M.; Li, H.; Chen, H. High Efficiency Hybrid Solar Cells Using Post-Deposition Ligand Exchange by Monothiols. *Phys. Chem. Chem. Phys.* **2012**, *14* (35), 12094−12098.

(23) Qian, L.; Yang, J.; Zhou, R.; Tang, A.; Zheng, Y.; Tseng, T.-K.; Bera, D.; Xue, J.; Holloway, P. H. Hybrid Polymer-CdSe Solar Cells with a ZnO Nanoparticle Buffer Layer for Improved Efficiency and Lifetime. *J. Mater. Chem.* **2011**, *21* (11), 3814−3817.

(24) Zhou, R.; Stalder, R.; Xie, D.; Cao, W.; Zheng, Y.; Yang, Y.; Plaisant, M.; Holloway, P. H.; Schanze, K. S.; Reynolds, J. R.; Xue, J. Enhancing the Efficiency of Solution-Processed Polymer:Colloidal Nanocrystal Hybrid Photovoltaic Cells Using Ethanedithiol Treatment. *ACS Nano* **2013**, *7* (6), 4846−4854.

(25) Liu, Y.; Gibbs, M.; Puthussery, J.; Gaik, S.; Ihly, R.; Hillhouse, H. W.; Law, M. Dependence of Carrier Mobility on Nanocrystal Size and Ligand Length in PbSe Nanocrystal Solids. *Nano Lett.* **2010**, *10* (5), 1960−1969.

(26) Barkhouse, D. A.; Pattantyus-Abraham, A. G.; Levina, L.; Sargent, E. H. Thiols Passivate Recombination Centers in Colloidal Quantum Dots Leading to Enhanced Photovoltaic Device Efficiency. *ACS Nano* **2008**, *2* (11), 2356−2362.

(27) Luther, J. M.; Law, M.; Song, Q.; Perkins, C. L.; Beard, M. C.; Nozik, A. J. Structural, Optical, and Electrical Properties of Self-Assembled Films of PbSe Nanocrystals Treated with 1,2-Ethanedithiol. *ACS Nano* **2008**, *2* (2), 271−280.

(28) Bisri, S. Z.; Piliego, C.; Yarema, M.; Heiss, W.; Loi, M. A. Low Driving Voltage and High Mobility Ambipolar Field-Effect Transistors with PbS Colloidal Nanocrystals. *Adv. Mater.* **2013**, *25* (31), 4309−4314.

(29) Jarzab, D.; Cordella, F.; Lenes, M.; Kooistra, F. B.; Blom, P. W.; Hummelen, J. C.; Loi, M. A. Charge Transfer Dynamics in Polymer-Fullerene Blends for Efficient Solar Cells. *J. Phys. Chem. B* **2009**, *113* (52), 16513−16517.

DOI: 10.1021/acsami.5b04550
ACS Appl. Mater. Interfaces 2015, 7, 19083−19090

(30) Kwon, S.; Lim, K.-G.; Shim, M.; Moon, H. C.; Park, J.; Jeon, G.; Shin, J.; Cho, K.; Lee, T.-W.; Kim, J. K. Air-Stable Inverted Structure of Hybrid Solar Cells Using a Cesium-Doped ZnO Electron Transport Layer Prepared by a Sol-Gel Process. *J. Mater. Chem. A* **2013**, *1* (38), 11802−11808.
(31) Malizia, M.; Seger, B.; Chorkendorff, I.; Vesborg, P. C. K. Formation of a P-N Heterojunction on GaP Photocathodes for H_2 Production Providing an Open-Circuit Voltage of 710 mV. *J. Mater. Chem. A* **2014**, *2* (19), 6847−6853.
(32) Lee, M. H.; Takei, K.; Zhang, J.; Kapadia, R.; Zheng, M.; Chen, Y. Z.; Nah, J.; Matthews, T. S.; Chueh, Y. L.; Ager, J. W.; Javey, A. P-type InP Nanopillar Photocathodes for Efficient Solar-Driven Hydrogen Production. *Angew. Chem., Int. Ed.* **2012**, *51* (43), 10760−10764.
(33) Dai, P.; Li, W.; Xie, J.; He, Y.; Thorne, J.; McMahon, G.; Zhan, J.; Wang, D. Forming Buried Junctions to Enhance the Photovoltage Generated by Cuprous Oxide in Aqueous Solutions. *Angew. Chem., Int. Ed.* **2014**, *53* (49), 13493−13497.
(34) Lin, Y.; Battaglia, C.; Boccard, M.; Hettick, M.; Yu, Z.; Ballif, C.; Ager, J. W.; Javey, A. Amorphous Si Thin Film Based Photocathodes with High Photovoltage for Efficient Hydrogen Production. *Nano Lett.* **2013**, *13* (11), 5615−5618.
(35) Haro, M.; Solis, C.; Molina, G.; Otero, L.; Bisquert, J.; Gimenez, S.; Guerrero, A. Toward Stable Solar Hydrogen Generation Using Organic Photoelectrochemical Cells. *J. Phys. Chem. C* **2015**, *119* (12), 6488−6494.
(36) Dotan, H.; Sivula, K.; Grätzel, M.; Rothschild, A.; Warren, S. C. Probing the Photoelectrochemical Properties of Hematite (α-Fe_2O_3) Electrodes Using Hydrogen Peroxide as a Hole Scavenger. *Energy Environ. Sci.* **2011**, *4* (3), 958−964.
(37) Fabregat-Santiago, F.; Garcia-Belmonte, G.; Mora-Sero, I.; Bisquert, J. Characterization of Nanostructured Hybrid and Organic Solar Cells by Impedance Spectroscopy. *Phys. Chem. Chem. Phys.* **2011**, *13* (20), 9083−9118.
(38) Salvador, P.; Gutiérrez, C. Analysis of the Transient Photocurrent-Time Behaviour of a Sintered N-$SrTiO_3$ Electrode in Water Photoelectrolysis. *J. Electroanal. Chem. Interfacial Electrochem.* **1984**, *160* (1−2), 117−130.

DOI: 10.1021/acsami.5b04550
ACS Appl. Mater. Interfaces 2015, 7, 19083−19090